Atherosclerosis 304 (2020) 9–21

Contents lists available at ScienceDirect

Atherosclerosis

journal homepage: www.elsevier.com/locate/atherosclerosis

Dietary sucrose induces metabolic inflammation and atherosclerotic cardiovascular diseases more than dietary fat in *LDLr*$^{-/-}$ *ApoB*$^{100/100}$ mice

Laís R. Perazza[a,b], Patricia L. Mitchell[a,b,1], Benjamin A.H. Jensen[a,c,1], Noëmie Daniel[a,b], Marjorie Boyer[a], Thibault V. Varin[a,b], Rihab Bouchareb[a,2], Renato T. Nachbar[a], Michaël Bouchard[d], Mylène Blais[d], Andréanne Gagné[a], Philippe Joubert[a], Gary Sweeney[e], Denis Roy[b], Benoit J. Arsenault[a], Patrick Mathieu[a], André Marette[a,b,*]

[a] Quebec Heart and Lung Institute, Department of Medicine, Faculty of Medicine, Laval University, Quebec City, Quebec, Canada
[b] Institute of Nutraceuticals and Functional Foods, Laval University, Quebec City, Quebec, Canada
[c] Novo Nordisk Foundation Center for Basic Metabolic Research, Section for Human Genomics and Metagenomics in Metabolism, Faculty of Health and Medical Sciences, University of Copenhagen, Copenhagen, Denmark
[d] Sherbrooke Research and Development Centre, Agriculture and Agri-Food, Canada, Sherbrooke, Québec, Canada
[e] Department of Biology, York University, Toronto, Ontario, Canada

HIGHLIGHTS

- High-fat feeding promotes more obesity and insulin resistance than sucrose intake.
- Sucrose intake lowers gut microbial diversity and increases bowel inflammation.
- Sucrose, not fat, is the main dietary driver of atherosclerosis and LV enlargement.
- Dietary sucrose causes higher hepatic inflammation and fibrosis than fat feeding.

ARTICLE INFO

Keywords:
Sugar
Fat
Obesity
Inflammation
Insulin resistance
CVD

ABSTRACT

Background and aims: Poor dietary habits contribute to the obesity pandemic and related cardiovascular diseases but the respective impact of high saturated fat *versus* added sugar consumption remains debated. Herein, we aimed to disentangle the individual role of dietary fat *versus* sugar in cardiometabolic disease progression.
Methods: We fed pro-atherogenic *LDLr*$^{-/-}$ *ApoB*$^{100/100}$ mice either a low-fat/high-sucrose (LFHS) or a high-fat/low-sucrose (HFLS) diet for 24 weeks. Weekly body weight gain was registered. 16S rRNA gene-based gut microbial analysis was performed to investigate gut microbial modulations. Intraperitoneal insulin (ipITT) and oral glucose tolerance test (oGTT) were conducted to assess glucose homeostasis and insulin sensitivity. Cytokines were assessed in fasted plasma, epididymal white adipose tissue and liver lysates. Heart function was evaluated by echocardiography. Aortic atheroma lesions were quantified according to the *en face* technique.
Results: HFLS feeding increased obesity, insulin resistance and dyslipidemia compared to LFHS feeding. Conversely, high sucrose consumption decreased gut microbial diversity while augmenting inflammation and the adaptative immune defense against metabolic endotoxemia and reduced macrophage cholesterol efflux capacity. This led to more severe cardiovascular complications as revealed by remarkably high level of atherosclerotic lesions and the early development of cardiac dysfunction in LFHS *vs* HFLS fed mice.
Conclusions: We uncoupled obesity-associated insulin resistance from cardiovascular diseases and provided novel evidence that dietary sucrose, not fat, is the main driver of metabolic inflammation accelerating severe atherosclerosis in hyperlipidemic mice.

* Corresponding author.Laval Hospital. 2700, Chemin Quatre-Bourgeois, room Y4340 Québec, G1V 4G5, Canada.
E-mail address: andre.marette@criucpq.ulaval.ca (A. Marette).
[1] These authors contributed equally to this work.
[2] Current affiliation: Icahn School of Medicine, Department of cardiology, Mount Sinai. New York, 10029. USA

https://doi.org/10.1016/j.atherosclerosis.2020.05.002
Received 5 November 2019; Received in revised form 12 April 2020; Accepted 7 May 2020
Available online 24 May 2020

1. Introduction

Cardiovascular diseases (CVD) are the leading cause of mortality worldwide, accounting for one third of global deaths [1]. Robust scientific evidence links metabolic dysfunction to CVD development, where altered lipid metabolism represents an independent risk factor of atherosclerosis [2]. As such, lipid-lowering therapy remains the principal target for atherosclerotic CVD management [3]. Yet, the progressive and multifactorial nature of CVDs, including atherosclerosis, is not fully elucidated.

While poor dietary habits and excess caloric intake are key drivers of the obesity epidemic and related CVDs, the distinct role of excess fat *versus* added sugar consumption remains debatable. The centric view that dietary fat is the main culprit for excess body weight and CVDs [4] is still controversial and may limit our understanding of metabolic adaptations [5] in the context of excessive calorie consumption. Indeed, epidemiological studies suggest that neither total fat intake nor the type of dietary fat associates with CVD risk or mortality [6,7]. In contrast, mounting evidence points towards added sugar consumption paralleling obesity and T2D development [8–11] along with non-alcoholic fatty liver disease (NAFLD) [12].

Chronic low-grade inflammation is a prominent feature of obesity and a central player in the development of cardiometabolic diseases [4,13]. A growing body of evidence indicates that obesity-linked inflammation, also known as metabolic inflammation, associates with gut microbiota perturbations disturbing host metabolism [14]. Indeed, high caloric consumption through high intake of saturated fat and sugar has been shown to promote gut dysbiosis and to decrease gut integrity, thus facilitating host exposure to microbial-derived inflammatory factors, which contributes to metabolic endotoxemia and insulin resistance [14,15]. Still, it remains unclear whether dietary fat and sucrose trigger similar shifts in gut microbial populations and related inflammatory disturbances in key metabolic tissues.

In the present study, we aimed to compare the selective effects of a high intake of fat or sucrose in pro-atherogenic $LDLr^{-/-}$ $ApoB^{100/100}$ mice to tease out their independent contribution to the development of cardiometabolic disorders. We found that high fat intake induced more obesity, insulin resistance and hepatic lipid accumulation than high sugar intake. In contrast, excessive dietary sucrose consumption enhanced adipose, liver and intestinal inflammation concomitant with reduced gut microbiota diversity and increased both mucosal and systemic adaptative immune defense against endotoxemia. Most importantly, sucrose-induced inflammation also promoted greater atherosclerotic plaque formation and left ventricular enlargement, which was potentially mechanistically linked with reduced high-density lipoprotein (HDL)-mediated cholesterol efflux capacity.

2. Materials and methods

2.1. Animals

$LDLr^{-/-}/ApoB^{100/100}$ mice were generated from original founders kindly provided by Drs. Seppo Ylä-Herttuala and Markku Laakso (Kuopio University, Kuopio, Finland) and backcrossed on a C57BL/6J background from Jackson Laboratories (Bar Harbor, ME). This genetic mouse model was chosen since wild type mice do not express cholesteryl ester transfer protein (CETP), which is an important enzyme responsible for the exchange of triglycerides (TG) from very low-density lipoproteins (VLDL) and low-density lipoprotein (LDL) to cholesterol-esters of HDL in humans [16]. The exclusive role of HDL in the reverse cholesterol transport of mice, provides a natural resistance to atherosclerosis development. LDL receptor knockout ($LDLr^{-/-}$) mice are largely used for investigating the impact of diets and drugs on the development of atheroma lesions. Moreover, ApoB-48 is a truncated version of the ApoB-100 protein that results from a premature stop codon in the *ApoB* gene [17]. Rodents are able to produce both proteins in the liver, while humans synthetize only ApoB-100. Therefore, to target a more humanized dyslipidemic profile, we have selected transgenic $LDLr^{-/-}$ mice expressing only ApoB-100 in the liver.

Eight-week-old male $LDLr^{-/-}/ApoB^{100/100}$ mice were housed individually at the Quebec Heart and Lung Institute facility on a regulated day/light cycle. Animals had free access to food and water for 2 weeks of acclimation on chow diet (Teklad 2018, Harlan) before they were randomly divided into the following experimental groups. Mice were fed either a low-fat/high-sucrose (LFHS) diet containing 14% of total kcal from lipids (1:1 corn oil to lard ratio) and 73% from carbohydrates (sucrose; Supplementary Table 1), or a high-fat/low-sucrose (HFLS) diet containing 65% of kcal from lipids (1:1 corn oil to lard ratio) and 22% from carbohydrates (sucrose; Supplementary Table 1). Both diets contained 12% of kcal of proteins from various sources (*e.g.* 10% eggs, 10% soya, 53% beef and 27% chicken) based on published human consumption data [18]. In order to accelerate the atherosclerotic process, 0.2% cholesterol (w/w) was added to both diets. Body weight gain was measured once per week. Food intake in grams was measured three times a week (LFHS diet 3.90 kcal/g and HFLS diet 5.51 kcal/g (Supplementary Table 1), with energy excretion being calculated (Supplementary Table 2). Following 24 weeks of diet treatment, fasted mice were anesthetized with isoflurane and euthanized by cardiac puncture. Epididymal and retroperitoneal white adipose tissue (eWAT and rpWAT, respectively), liver, jejunum, ileum, colon, gastrocnemius and soleus muscles as well as heart were snap frozen in liquid nitrogen. Caecum content was weighted and colon length measured. The aorta was fixed in 4% paraformaldehyde/PBS solution and subsequently kept in 1% PBS solution for further analysis. Animal protocols were approved by the Animal Care Committee of Laval University.

2.2. Insulin and glucose tolerance test

After 17 weeks on experimental diets, animals were fasted 6 h prior to an intraperitoneal injection of insulin (0.65 U/Kg) to assess insulin tolerance (ipITT). Glycaemia was measured before and 5, 10, 15, 20, 30 and 60 min after insulin injection. An oral glucose tolerance test (oGTT) was performed on 12 h-fasted mice at week 19 following a glucose gavage of 1 g/kg of body weight. Glycaemia was assessed with a One Touch Ultra glucometer (LifeScan, Inc.) before and after 15, 30, 60, 90 and 120 min. Blood samples were also collected at each time point for insulin determination. The homeostasis model assessment of insulin resistance index (HOMA-IR) was calculated based on the formula: fasting insulinemia (μUI/mL) x fasting glycemia (mM)/22.5. Matsuda insulin sensitivity index was calculated as previously described [19].

2.3. Analytical methods

In order to assess fed-state plasma lipid profiles, mice were fasted for 12 h after 12 weeks of treatment and then refed for 1 h followed by blood collection. Blood was collected in EDTA-coated tubes, centrifuged and plasma was kept at −80 °C for further analysis. Standard colorimetric kits were used for assessment of TG (TR22421; Thermo Scientific), cholesterol (CH200; Randox), HDL (CH2652; Randox), LDL (CH2657; Randox) and oxidized-LDL (oxLDL; MBS703519; MyBio Source) in plasma from re-fed mice. In the fasting state, TG, cholesterol and HDL were measured by the biochemistry department of the Heart and Lung Institute of Laval University by calorimetry using the Siemens Dimension Vista® 1500 system. LDL was calculated using the Friedewald equation. Fasting blood urea nitrogen was analyzed by photometry using the same analytic system. Insulin concentration was measured in plasma collected during oGTT with the use of the Ultrasensitive mouse ELISA kit (EMD Millipore). High-molecular weight (HMW) adiponectin was measured in fasted plasma using an ELISA kit (MBS028367; MyBioSource). Plasma and tissue cytokines and chemokines were measured in the fasted state using a Bio-plex pro assay (10014905; Bio-Rad Laboratories). Circulating adhesion

molecules were measured by a Milliplex map kit assay (MCVD1MAG-77K; Millipore Sigma) whereas vascular cell adhesion molecule-1 (VCAM-1) was assessed by a quantitative ELISA kit (MVC00; R&D systems). Plasma lipopolysaccharide (LPS) – a component of outer membrane of Gram-negative bacteria – was measured by a quantitative ELISA kit (MBS700021; MyBioSource). Systemic (anti-IgG; 375112, GE) and mucosal (anti-IgA; 14-10- 01, KPL) immunomodulatory response to LPS and flagellin were measured by quantitative ELISA in a 96- well plate coated with 100 μL of either LPS (from *E. coli* 0128: B12; 2887, Sigma) or flagellin (from *Salmonella enterica* subsp. *enterica serovar Typhimurium* str. LT2, SRP8029, Sigma), respectively. Liver TGs were measured by an adaptation of the Folch method [20]. To calculate energy excretion, 24-hour fecal energy content was estimated by the heat of combustion using a calorimetric bomb.

2.4. Histological analysis of adipose tissue and liver

At necropsy, portions of eWAT and liver were isolated and fixed in 4% paraformaldehyde/PBS solution. Tissues were embedded with paraffin, sectioned (4 μm) and stained with hematoxylin and eosin (H& E). Adipocyte size was measured in eWAT stained with H&E as described previously [21]. Liver sections were evaluated blindly by two pathologists using a scoring system proposed by Liang et al. [22]. Briefly, steatosis score was given according to the percentage of hepatocytes with hypertrophy (defined as hepatocytes 1.5-fold larger than normal), macro and microvascular steatosis. For each of the three steatosis features, 5–33% was attributed a score of 1, 33–66% a score of 2 and more than 66% a score of 3. Livers in which the sum of scores from the three features resulted in a total score greater than 3 were diagnosed as NAFLD. Hepatic inflammation was determined based on the number of inflammatory foci (cluster of five or more inflammatory cells) per field at 10X magnification (3.5 mm^2) in at least five independent fields. In addition to NAFLD features, 0.5 foci per field was considered positive for nonalcoholic steatohepatitis (NASH) diagnosis.

Hepatic fibrosis was assessed on Sirius red stained slides as previously described [23,24]. Briefly, slides were deparaffinized for 5 min in toluene followed by a graded ethanol series. Then, an 8-minute incubation with Weigert's hematoxyline was performed followed by a 1h-staining with 0.1% Sirius red/picric acid isopropyl alcohol (picro-Sirius red solution). Excess picro-Sirius red solution was washed out using acidified water for later dehydration (100% ethanol) followed by toluene finalization. Fibrosis was scored according to the Kleiner et al. classification [25]: Fibrosis located on perisinusoidal or periportal regions was categorized as a score of 1, fibrosis in both regions as a score of 2, bridging fibrosis conformation as a score of 3 and cirrhosis as a score of 4.

2.5. Atherosclerosis determination

Atheroma lesions were quantified according to the *en face* technique [26] in dissected and stained aorta from 2 thirds of mice for each group, randomly selected. Briefly, excised aortas were stored under 4 °C in 5% formalin. Perivascular adipose tissue was removed, and the aorta was bisected exposing the intima layer. The aorta was then pinned *en face* and stained with 0.5% Sudan IV. Images were captured using a camera attached to a Leica MZ6 dissecting microscope. Atherosclerosis severity was estimated as a percentage of atherosclerotic lesion area corrected by the total aortic area with the use of ImageJ software (V. 1.51j8, NIH, USA).

2.6. Histological analysis of aortic inflammation and oxidative stress

Aorta from the *en face* preparation were rolled into a spiral-like Swizz-roll, placed in a cassette and stored in 4% paraformaldehyde/PBS solution. Tissues were embedded with paraffin and sectioned (4 μm). Immunohistochemistry of aortic sections was performed using an ABC-peroxidase kit (Vector laboratories, VECTPK400). Briefly, after inhibiting endogenous peroxidase (Dako REAL peroxidase-blocking solution, S202386-2), tissues were incubated with TBS-BSA 5% for 30 min and then incubated overnight with the primary antibody against integrin alpha M subunit (CD11b, 1:100, Abicam, ab133357), cluster of differentiation 68 (CD68, 1:100, Abcam, ab31630), inducible nitric oxide synthase (iNOS, 1:100, Cell signaling, 2982) and nuclear factor kappa-light-chain-enhancer of activated B cells (NFkB, 1:400, Abcam, ab31409). Slides were then incubated with the appropriate biotinylated secondary antibody for 1 h. Next, aortic tissues reacted with the ABC-HRP solution (Vector laboratories, VECTPK400) for 40 min to later staining using DAB peroxidase substrate solution (Vector laboratories, SK-4100). Hematoxylin was added to each slide, as a counterstain for 30 s and rinsed in water. Blind analyses were performed on a high-power resolution field, 50% zoom, acquired in Axio Observer.Z1 (Zeiss) using a Plan- Apochromat 20x objective. Staining quantification was made using the software Image J 1.52p (NIH, USA).

Aorta from the remaining one third of mice from each group were harvested at euthanasia and assigned for qPCR and oxidative stress evaluation. The posterior 3–4 cm portion of aorta were immediately frozen in OCT and later cut in 14 μm. OCT sections were thawed and kept under phosphate buffer (0,1 M; pH 7,4) with $CaCl_2$ (0,45 mM) for 10 min at 37 °C. Slides were incubated in oxidative fluorescent dihydroethidium (DHE, 2 Mm, Life Technologies) containing buffer. Superoxide anion ($O2^{\bullet-}$) production was estimated by the DHE fluorescence intensity in images taken with an Axio Observer.Z1 (Zeiss) using a Plan-Apochromat 20x objective. Fluorescence quantification was performed by mean of fluorescent intensity in multiple sections taken randomly along intimal layer (Image J, NIH, USA).

2.7. Cholesterol efflux capacity

Cholesterol efflux from J774 macrophages was assessed by radiolabeled cholesterol efflux quantification after ApoB-depleted plasma incubation. Briefly, J774 macrophages were plated and incubated for 24 h with media containing 1% bovine growth serum and 2 μCi of ^{3}H-cholesterol/ml, as previously described [27]. Following a 4 h incubation with 2% plasma depleted of ApoB with 40% polyethylene glycol-6000, media was collected and cells were harvested in 0.5 N NaOH. Radiolabeled ^{3}H-cholesterol efflux from macrophages mediated by HDL was calculated as follows: [counts per minutes (cpm) in media/(cpm in media + cpm in cell lysates)]. The latter was subtracted from cholesterol efflux capacity using plasma from the studied mice.

2.8. Echocardiography and blood pressure

Transthoracic echocardiography was performed at weeks 0, 12 and 24 under isoflurane anesthesia with the L15-7io (5–12 Megaherz) and S12-4 (4–12 Megaherz) probes connected to a Philips HD11XE ultrasound system (Philips Healthcare Ultrasound, The Netherlands) as previously described [28]. In short, left ventricular (LV) dimensions: LV interior diameter at end-diastole (LVIDd), LV relative wall thickness (LVRWT) and LV outflow-tract diameter (LVOT) were acquired in M-mode imaging of parasternal short-axis view. Fractional shortening (LVFS), ejection fraction (EF) and LV mass calculations were based on LV dimensions as previously [28]. Transmitral (A and E wave) and LVOT flow velocity were accessed by pulsed-wave Doppler and mitral annulus motion velocity (E′ wave) by Doppler tissue imaging. Stroke volume (SV) was based on LVOT flow velocity and cardiac output (CO) was estimated by the product of SV and heart rate (HR).

At week 24, we assessed arterial blood pressure by using a non-invasive CODA tail-cuff system. Briefly, the experiment was conducted in 26 °C and after 5 min of acclimation inside the apparatus, 20 consecutives cycles of blood pressure measurements were taken, while the first 5 were excluded. Systolic, diastolic and mean blood pressure were acquired.

2.9. 16S rRNA gene-based gut microbial analysis

Fresh fecal samples were collected at weeks 12 and 24 and stored at −80 °C. Bacterial genomic DNA was extracted using a DNA extraction kit (DNeasy, Qiagen). Extracted DNA was stored at −20 °C until further analysis. 16S rRNA amplification and fecal microbiota profiling were acquired as previously described [29,30].

2.10. Fecal short-chain fatty (SCFA) acid profiling

Fecal SCFAs were quantified using gas chromatography/mass spectrometry (GC/MS). Briefly, 80–100 mg of feces were rapidly frozen under 0.5% of acid phosphoric solution for further analysis. Homogenized samples were centrifuged at 4 °C at 17,949*g* for 10 min. 600 µl of supernatants was transferred into a tube containing a 20 mM solution of 4-methylvaleric acid, acetic acid, propionic acid, isobutyric acid, butyric acid, isovaleric acid and valeric acid (Sigma- Aldrich) in ethyl acetate (Sigma-Aldrich). Samples were then mixed and centrifuged at 4 °C at 1740*g* for 2 min. Analysis were performed on 200 µL of supernatant on a GC-2010 Plus (Shimadzu) with an autosampler AOC-20s, AOC-20i injector and FID detector.

2.11. Real-time polymerase chain reaction

Total RNA was isolated from homogenized jejunum, ileum, colon, liver and aorta using a GeneJETRNA purification kit (Thermofisher, Canada), while RNeasy fibrous tissue kit (Qiagen, Canada) was used for the heart. One microgram of RNA was reverse transcribed using the High Capacity cDNA Reverse Transcription Kit (Applied Biosystems, Canada) and Quantitative real-time PCR (qPCR) was performed with Quantitec SYBR Green PCR kit (Qiagen, Canada) on the Rotor-Gene 6000 system (Corbett Robotics Inc., CA, USA).

2.12. Statistical analyses

Data were tested for Gaussian distribution and subsequently assessed by Student's *t*-test or non-parametric Mann Whitney *U* test, as appropriate, to calculate significance levels between groups (GraphPad, USA). Body weight gain, ipITT, oGTT, insulinemia during oGTT and Shannon index were statistically compared using two-way repeated measures ANOVA with a Dunnett post hoc test (Sigmaplot, USA). Statistical differences on dietary-modulated taxa and predicted function was tested using linear discriminant analysis (LDA) effect size [31] (LEfSe). LDA threshold was set at 2.5 and statistical significance was established after factorial Kruskal–Wallis rank-sum test. All results were considered statistically significant at $p < 0.05$.

3. Results

3.1. Reduced gut microbial diversity in mice fed high sucrose is concomitant with exaggerated intestinal inflammation and metabolic endotoxemia

Under homeostatic conditions, host-gut microbiome symbiosis is mutually beneficial [32]. Gut dysbiosis, induced by poor dietary habits and characterized by reduced microbial diversity and/or altered composition negatively, impacts host metabolism [33]. The specific effects of excessive consumption of fat *versus* sucrose on gut microbiota taxonomic profile were evaluated by 16S rRNA gene-based amplicon sequencing in fecal samples obtained at weeks 12 and 24.

LFHS-fed mice showed lower α-diversity (Fig. 1A) when compared to HFLS-fed and a distinct gut microbial community structure (Fig. 1B). Since obesogenic diets have been extensively associated with lower microbial diversity and higher Firmicutes to Bacteroidetes ratio [33–35], we next applied LEfSe to evaluate the most pronounced differentially abundant taxa. This analysis revealed that several SCFA-producing bacteria (*i.e. Lachnospiraceae*, *Rumino_Ruminococcus*, *Ruminococcaceae*, *Dorea*, *Oscillospira*, *Clostridiales, Coprococcus*) were underrepresented in LFHS-fed mice (Fig. 1C), hence potentially influencing gut ecology. This apparent decrease in SCFA producers in the gut microbiome of LFHS-fed mice paralleled a trend for diminishing levels of fecal valeric acid ($p = 0.051$; Fig. 1D) as compared to HFLS-fed, whereas acetic and propionic acids, despite not statistically significant, had an opposite modulation (Fig. 1D).

Augmented intestinal inflammation associated with bacterial encroachment increases LPS leakage from the gut lumen into the circulation potentially resulting in metabolic endotoxemia [14]. Dietary sucrose fueled intestinal inflammation as seen by an overall higher gene expression of *Il18* and *Ccl5* (Fig. 2A–C). Interestingly, animals fed with high sucrose diet had a 10-fold higher expression level of regenerating islet-derived (Reg)-3 (β and γ isoforms) in both jejunum and ileum (Fig. 2A and B). Reg3β and Reg3γ are antimicrobial peptides known to be upregulated in chronic mucosal inflammation as an early defense mechanism against pathogens [36,37]. We also observed a ~2-fold higher gene expression of mucin 2 (*Muc2*) in ileum and a trend in jejunum ($p = 0.06$) of LFHS-fed mice (Fig. 2A and B) and a ~5-fold higher expression of inducible nitric oxide (NO) synthase (*Nos2*; Fig. 2A–C) in all analyzed intestinal sections followed LFHS consumption. iNOS is a well-known inflammatory mediator through its ability to release high NO levels and implicated in epithelial injury processes [38]. Thus, quantitative gene expression results suggest activation of an intestinal innate immune response following high sucrose feeding. Accordingly, LFHS-feeding resulted in colon shortening, a typical histopathological alteration observed in inflammatory bowel disease [39], when compared to HFLS-fed mice (Fig. 2D). Likewise, despite similar levels of total circulating LPS (Fig. 2E), LFHS-fed mice displayed higher plasma IgG as well as IgA antibody titers against this gram-negative bacterial cell wall component (Fig. 2F and G). Similarly, plasma anti-flagellin (protein from the bacterial flagellum) IgG also showed a trend to be higher in sucrose-fed mice ($p = 0.07$; Fig. 2H). Combined, IgG and IgA-mediated anti-bacterial defense products suggest increased bacterial encroachment accompanied by enhanced immunoreactivity of both systemic and mucosal nature [40].

3.2. Distinct impact of dietary sucrose and fat on body weight gain, adipose tissue inflammation and insulin resistance

While energy intake did not differ between groups (Fig. 3A), body weight was significantly higher for the HFLS-fed mice starting at 5 weeks of treatment and this difference persisted until week 24 (Fig. 3B) resulting in a 3-fold increase in visceral obesity (Supplementary Table 2). HFLS-fed mice had slightly lower energy excretion (Supplementary Table 2). Despite less visceral fat accumulation (Supplementary Table 2) and smaller mean adipocyte size (Fig. 3C), LFHS-fed mice exhibited increased adipose inflammation as revealed by higher protein levels of tumor necrosis factor-α (TNF-α), interferon-γ (IFN-γ) and interleukin-6 (IL-6) and a trend ($p = 0.083$) for greater interleukin-1β (IL- 1β) levels in eWAT (Fig. 3D), hence countering the assumption that the level of adipose tissue inflammation follows the accumulation of visceral fat. The levels of chemoattractant proteins (MCP-1, RANTES; Fig. 3D) and circulating HMW-adiponectin levels (Supplementary Table 2) did not differ between groups.

We next evaluated the impact of the two diets on glucose homeostasis and insulin sensitivity. Although no differences were noted in glycemia during oGTT (Supplementary Table 2 and Fig. 3E), HFLS-fed animals exhibited much higher fasting (Supplementary Table 2) and post-glucose challenge insulinemia (Fig. 3F). In addition, the HFLS group had higher glucose levels during ipITT starting 10 min after insulin injection (Fig. 3G), indicating decreased insulin sensitivity in comparison to LFHS-fed animals. HOMA-IR and Matsuda insulin indices further confirmed that HFLS-feeding led to a more severe insulin resistance than LFHS feeding (Supplementary Table 2). Thus, insulin resistance was linked to obesity and fat cell size in mice consuming high

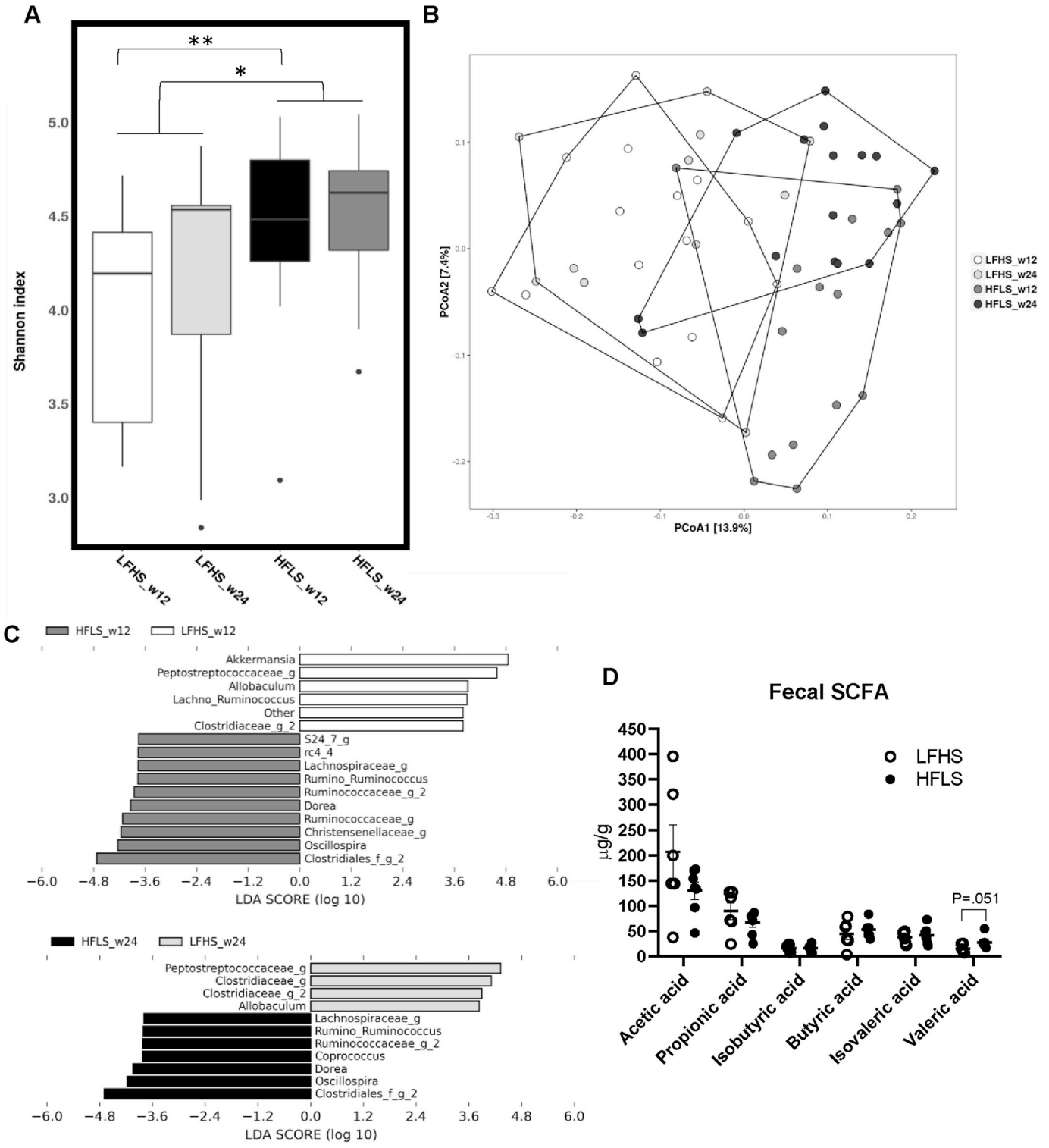

Fig. 1. Reduced gut microbial diversity and SCFA-producing bacteria relative abundance in mice fed high sucrose as compared to high fat.
Fecal samples were freshly harvested at week 12 and 24 for genomic DNA extraction and 16S rRNA-based analysis of the gut microbial profile was performed. Dietary effect on (A) α-diversity was estimated by the Shannon index and statistically tested by two-way repeated measures (RM) ANOVAs. Data are expressed by box-Whisker plots. (B) β-diversity is expressed by means of principal coordinate analysis (PCoA). (C) Relative abundance of taxa at the genus level was evaluated by linear discriminant analysis (LDA) at week 12 and week 24. LFHS n = 11/HFLS n = 16. Levels of (D) fecal SCFA were analyzed in fecal samples collected on week 24 and differences between groups were tested by Mann-Whitney, expressed as mean ± SEM. LFHS n = 7/HFLS n = 6."_f " and "_g" at the end of taxon refers to unidentified family and genus, respectively; SCFA: short-chain fatty acids.

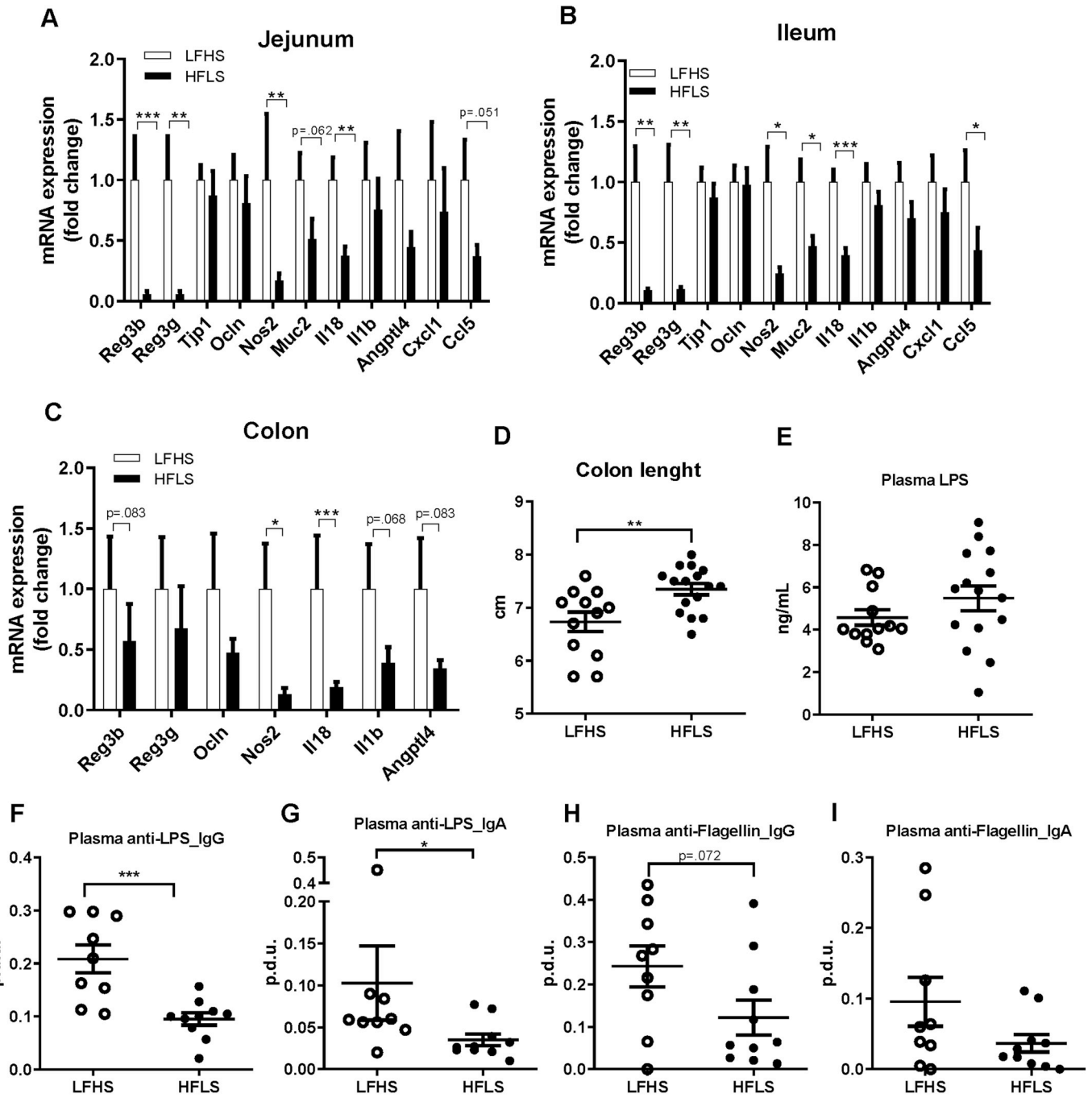

Fig. 2. High sucrose feeding exaggerated intestinal inflammation and metabolic endotoxemia as compared to high fat.
Jejunum, ileum and colon were collected during euthanasia for inflammatory cytokines gene expression quantification in (A) jejunum (LFHS n = 8/HFLS n = 11), (B) ileum (LFHS n = 8/HFLS n = 9) and (C) colon (LFHS n = 8/HFLS n = 10). (D) Colon length was measured with a ruler before snapped frozen (LFHS n = 12/HFLS n = 16). Metabolic endotoxemia was evaluated in fasted plasma (E) LPS level (LFHS n = 12/HFLS n = 15). Both, systemic (anti-IgG) and mucosal (anti-IgA) immune-defense (F and G) anti-LPS and (H and I) anti-flagellin were quantified in fasted plasma. LFHS n = 9/HFLS n = 10. Data are expressed as mean ± SEM. Student's *t*-test was applied to test the dietary effect in jejunum (*Tjp1, Il18*), ileum (*Reg3b*,*Reg3g*, *Ocln*, *Nos2*, *Muc2*, *Il18*, *Il1b*, *Angptl4*), LPS, anti-LPS_IgG and both anti-flagellin. Mann-Whitney test was used in jejunum (*Reg3b*,*Reg3g*, *Ocln*, *Nos2*, *Muc2, Il1b*, *Angptl4, Cxcl1, Ccl5*), ileum (*Tjp1, Cxcl1, Ccl5),* all colon genes and anti-LPS_IgA. $*p \leq .05$, $**p \leq .01$, $***p \leq .001$. LPS: Lipopolysaccharide; IgG: Immunoglobulin G; IgA: Immunoglobulin A.

fat diet, while adipose tissue inflammation was more associated with high sucrose feeding.

3.3. Dietary sucrose promotes higher liver inflammation and fibrosis and more macrovascular hepatic steatosis as compared to dietary fat

Concomitantly with higher visceral adiposity, HFLS-fed mice had increased liver weight and hepatic TG content compared to LFHS-fed animals (Fig. 4A and B). Yet, mirroring the findings from adipose tissue, LFHS-fed mice displayed greater overall liver inflammation (Fig. 4C), despite significantly less hepatic lipid accumulation.

The proinflammatory nature of sucrose rather than fat was confirmed by histological examination where 90% of LFHS-fed mice exhibited the highest inflammation score; a ~2-fold increase compared to HFLS-fed counterparts (Fig. 4D and E). Hepatic fibrosis scores accentuated this difference between groups, where we observed a ~4-fold

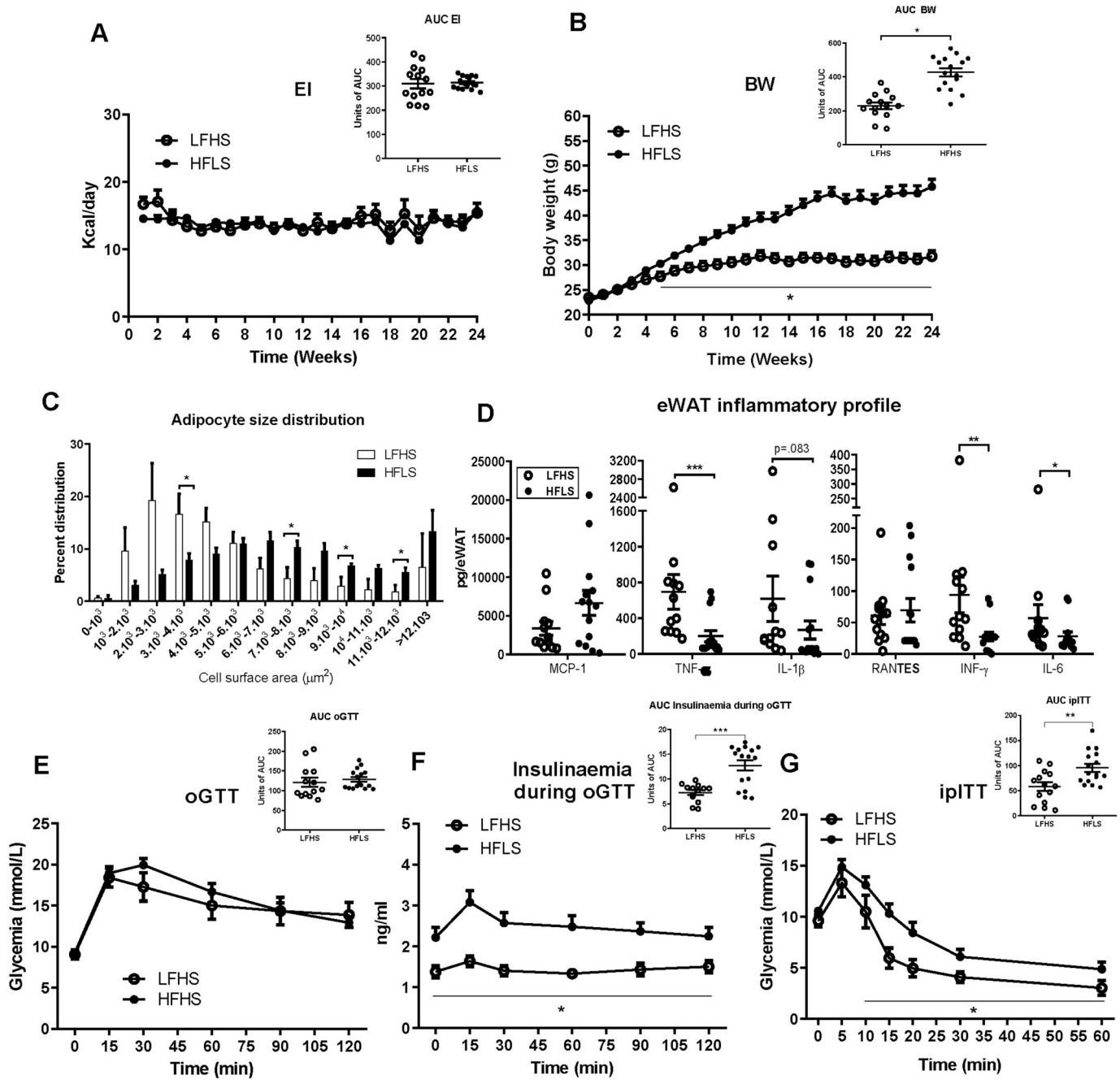

Fig. 3. Distinct impact of dietary sucrose and fat on body weight gain, adipose tissue inflammation and insulin resistance.
Mice were kept either on a LFHS or a HFLS diet for 24 weeks and eWAT was collected at euthanasia. Intraperitoneal insulin tolerance test (ipITT) and oral glucose tolerance test (oGTT) were performed at week 17 and 19, respectively. (A) EI and inserted AUC EI (LFHS n = 14/HFLS n = 16); (B) BW and inserted AUC BW (LFHS n = 14/HFLS n = 16); (C) adipocyte size distribution (LFHS n = 4/HFLS n = 5); (D) eWAT inflammatory profile (LFHS n = 12/HFLS n = 14); (E) oGTT and inserted AUC oGTT (LFHS n = 13/HFLS n = 16); (F) insulinaemia during oGTT and inserted AUC insulinaemia during oGTT (LFHS n = 13/HFLS n = 16); and (G) ipITT and inserted AUC ipITT (LFHS n = 14/HFLS n = 16). Data are expressed as mean ± SEM. Two-way repeated measures (RM) ANOVAs were applied to test dietary effect on EI, BW, oGTT, insulinaemia during oGTT and ipITT. *$p \leq .05$. Mann-Whitney test was applied to test dietary effect on adipocyte size distribution and eWAT-derived inflammatory profile. *$p \leq .05$, **$p \leq .01$, ***$p \leq .001$. Student's *t*-test was applied to test dietary effect on AUC EI, AUC BW, AUC oGTT, AUC insulinaemia during oGTT and AUC ipITT. *$p \leq .05$, **$p \leq .01$. EI: Energy intake; BW: Body weight; eWAT: Epididymal white adipose tissue; AUC: Area under the curve.

increase of LFHS- fed mice in the highest range compared to HFLS-fed counterparts (Fig. 4D–F). HFLS feeding was further associated with more prominent microvesicular steatosis, while LFHS-fed mice primarily presented macrovesicular steatosis, corroborating different pathophysiological features and hepatic adaptations to excess fat *versus* excess sugar (Fig. 4D and E).

3.4. Dietary sucrose intensifies atherosclerosis and LV chamber enlargement while reducing cholesterol efflux capacity

Dyslipidemia, a key determinant of cardiometabolic complications, was next analyzed in the fed and fasting state plasma. In the fed state, HFLS-fed mice had higher circulating TG and cholesterol, and lower HDL in comparison with the LFHS group (Fig. 5A). No differences were

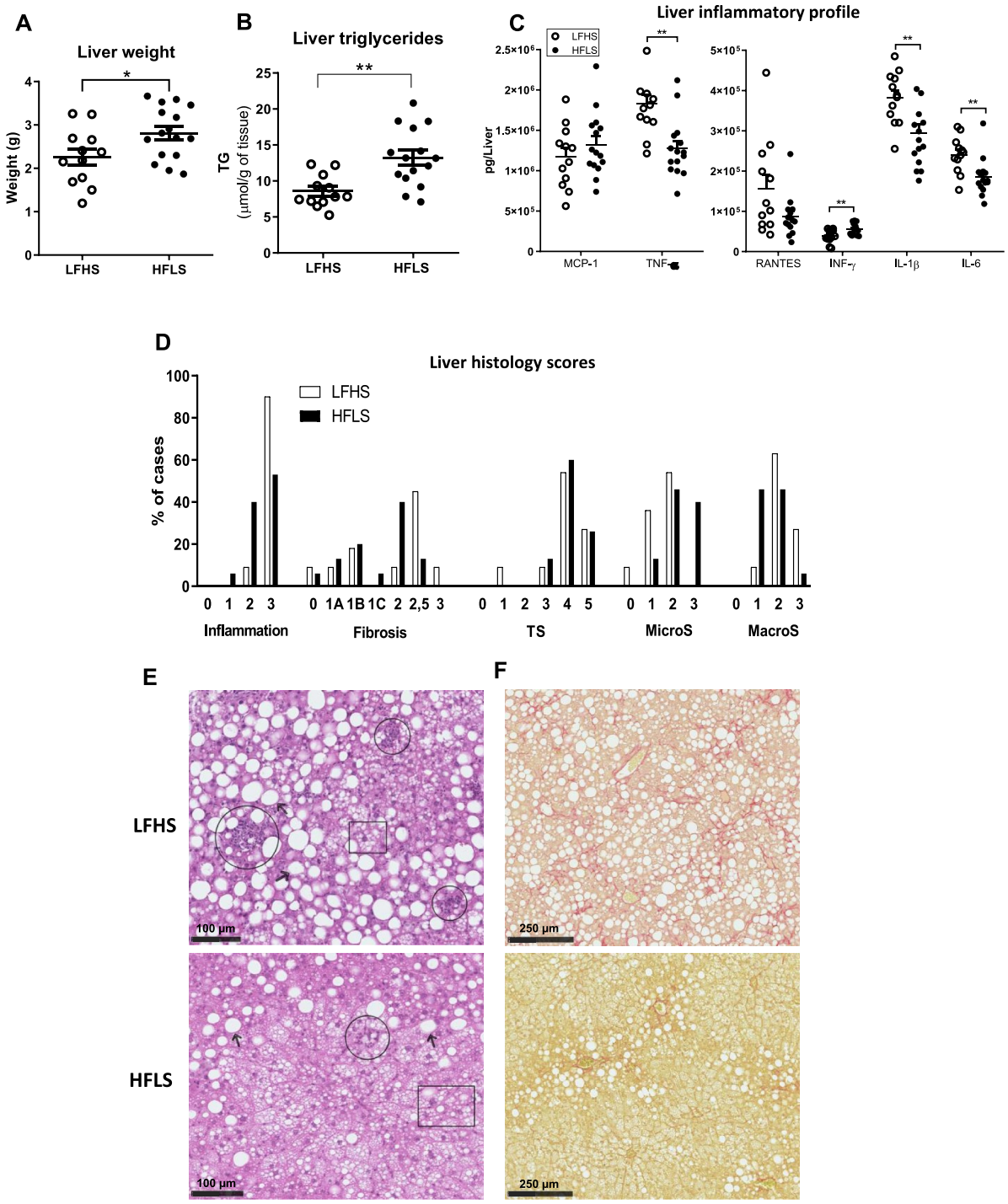

Fig. 4. Dietary sucrose promotes higher liver inflammation and fibrosis and more macrovascular hepatic steatosis as compared to dietary fat.
Liver was collected during euthanasia at week 24 for triglycerides and inflammatory cytokines quantification. (A) Liver weight (LFHS n = 12/HFLS n = 16); (B) liver triglycerides (LFHS n = 14/HFLS n = 15); (C) liver inflammatory profile (LFHS n = 12/HFLS n = 15); (D) liver histology scores (LFHS n = 11/HFLS n = 15); (E) representative images of liver H&E staining; (F) representative images of liver Sirius red staining. In figures A to C data are expressed as mean ± SEM, whereas in figure D data are presented as frequency of distribution. Student's *t*-test was applied to test dietary effect on liver weight, triglyceride and inflammatory cytokines. $^{*}p \leq .05$, $^{**}p \leq .01$. TS: Total steatosis; MicroS: Microvesicular steatosis; MacroS: Macrovesicularsteatosis. Black arrow: MacroS; Square: MicroS; Circle: Inflammatory foci.

noted for LDL or oxLDL levels between groups (Fig. 5A). Fasted mice from both dietary groups exhibited no differences in total circulating TG (Supplementary Fig. 2A), cholesterol (Supplementary Fig. 2B), LDL (Supplementary Fig. 2C) or HDL (Supplementary Fig. 2D). To further document the atheroprotective function of HDL, we next determined cholesterol efflux capacity from macrophages, the first and key step in the reverse cholesterol transport pathway, and a well-documented measure of HDL function [41,42]. Surprisingly, despite the greater plasma HDL-cholesterol content, LFHS-fed mice showed lower macrophage cholesterol efflux capacity in comparison with HFLS-fed mice (Fig. 5B). These data indicate that in a hyperlipidemic condition, a fat-rich diet is associated with more severe postprandial dyslipidemia than

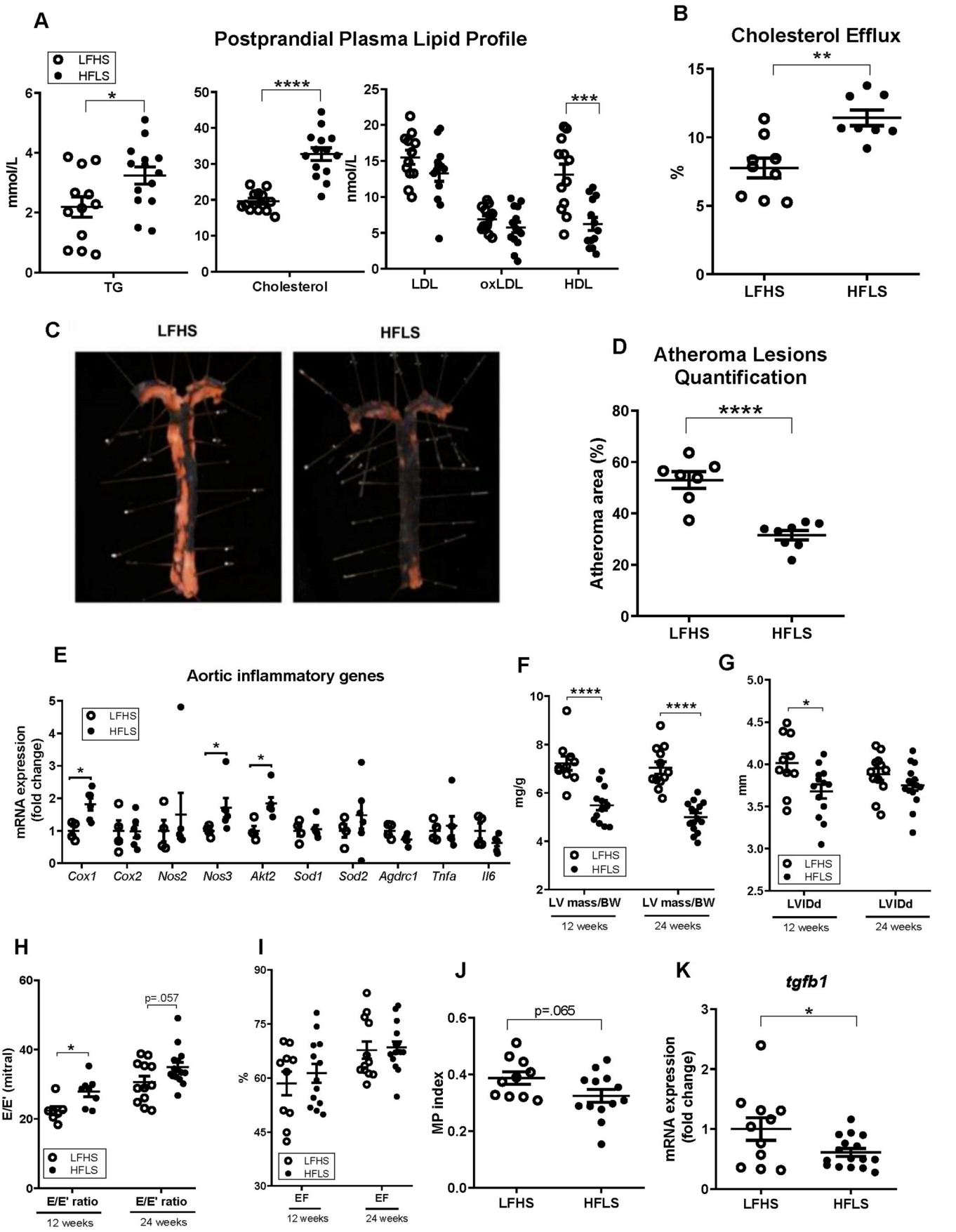

(caption on next page)

Fig. 5. Dietary sucrose intensifies atherosclerosis and LV chamber enlargement while reducing cholesterol efflux capacity.
Two thirds of the mice had the aortas harvested for atheroma lesions quantification according to the *en face* technique. Aortas from the remaining one third mice were collected for RNA isolation and further converted into cDNA to perform qPCR. ApoB-100 depleted plasma collected in a fasting-state at week 24 was used to quantify the cholesterol efflux capacity from macrophages. (A) Plasma lipid profile (LFHS n = 12/HFLS n = 14); (B) cholesterol efflux capacity (LFHS n = 9/HFLS n = 8); (C) representative images of *en face* aorta; (D) atherosclerosis quantification (LFHS n = 7/HFLS n = 8) and (E) aortic inflammatory genes (LFHS n = 4/HFLS n = 6). Data are expressed as mean ± SEM. Student's t-Test was applied to test dietary effect in plasma lipid profile, cholesterol efflux capacity, atherosclerosis quantification and cardiac *Tgfb1* expression. $*p \leq .05$, $**p \leq .01$, $***p \leq .001$, $****p \leq .0001$. Mann-Whitney test was applied to test the dietary effect on all aortic genes. Echocardiography study was performed at week 0, 12 and 24 to access cardiac function and left ventricle was isolated at euthanasia for qPCR. (F) LV-mass to BW; (G) LVIDd; (H) E/E' ratio; (I) EF; (J) MP index; (K) Cardiac Tgfb1 expression (LFHS n = 7-11/HFLS n = 12-16). Data are expressed as mean ± SEM and Student's t-Test was applied. $*p \leq .05$. LV: Left ventricle; BW: Body weight; LVIDd: Left ventricular interior diameter during diastole; E/E': Early (E) mitral flow velocity corrected by the early diastolic velocity (E') of medial mitral annulus; EF: Ejection fraction; MP: Myocardial performance.

a sucrose-rich diet, while the latter associates with reduced cholesterol efflux capacity.

We next assessed the impact of high fat *vs* high sucrose consumption on atherosclerotic lesions and found that LFHS-fed mice exhibited more severe atherosclerosis compared to HFLS-fed mice (Fig. 5C), which was confirmed by aortic lesion quantification (Fig. 5D). Atherosclerosis is a multifaceted disease involving inflammation, oxidative stress, and endothelial dysfunction [13]. Therefore, to elucidate potential sucrose-mediated pro-atherogenic mechanisms, we determined the expression of genes documented to be involved in this pathology. Along with advanced atherosclerosis, LFHS-feeding resulted in lower aortic gene expression of cyclooxygenase-1 (*Cox1*), endothelial nitric oxide synthase (eNOS; *Nos3*) and protein kinase B-2 (*Akt2*) as compared to HFLS-fed animals (Fig. 5E). Surprisingly, despite increased adipose and liver inflammation as well as a suggestive increase in plasma IL-1β ($p = 0.074$), E-selectin ($p = 0.076$) and vascular adhesion molecule 1 (VCAM-1; $p = 0.67$), LFHS-fed mice showed lower plasma MCP-1 (Supplementary Fig. 1A) and plasminogen activator inhibitor-1 (PAI-1; Supplementary Fig. 1B), while no differences were seen for the levels of TNF-α, RANTES, IL-6, intracellular cell adhesion molecule 1 (ICAM-1) and matrix metallopeptidase-9 (MMP-9; Supplementary Fig. 1A and B). We further evaluated oxidative stress via DHE fluorescence. DHE permeates the cell membrane and reacts with superoxide anion ($O_2^{\bullet-}$) producing ethidium, which intercalates with DNA, emitting a red fluorescence. No statistical differences on $O_2^{\bullet-}$ levels were observed between groups (Supplementary Fig. 3A and B). Aortic inflammation was further estimated by the positive staining of several inflammatory cell and cytokines markers by immunohistochemistry. Despite displaying ~80% enhanced atherosclerosis area, LFHS-fed mice did not show higher aortic inflammation as revealed by protein levels of CD11b, a protein expressed at the surface of many leukocytes (Supplementary Fig. 3C and D); CD68, a macrophage marker (Supplementary Fig. 3E and F); iNOS (Supplementary Fig. 3G and H) and NFkB (Supplementary Fig. 3I and J) in aortic sections.

Cardiac function was next assessed by echocardiography at baseline and after 12 and 24 weeks of dietary treatments (Supplementary Table 3). No differences were noted between groups at baseline (Supplementary Table 3). In line with the greater severity of atherosclerosis found in sucrose-fed animals, 12 weeks of LFHS diet elicited higher left ventricular (LV) mass, as well as higher LV interior diameter at the end of diastole (LVIDd) compared to HFLS group (Supplementary Table 3; Fig. 5F and G). No differences in LV right wall thickness (LVRWT) were noted between groups (Supplementary Table 3) and the ratio of early (E) mitral flow velocity corrected by the early diastolic velocity (E′) of medial mitral annulus (E/E′), an index of LV diastolic function, was lower in the LFHS group in comparison with the HFLS-fed animals (Supplementary Table 3 and Fig. 5H). LFHS-fed animals also showed increased myocardial performance (MP) index after 12 weeks (Fig. 5J), an index of global systolic and diastolic ventricular function [43]. Abnormal systolic function can prolong relaxation periods, which increases MP index thereby reducing mitral annular velocity (E/E'). Interestingly, such apparent cardiac dilation in LFHS fed mice may compensate the cardiac challenge since no changes were noticed on ejection fraction (EF; Supplementary Table 3 and Fig. 5I). A similar echocardiography profile was observed after 24 weeks on diet (Supplementary Table 3 and Fig. 5F–I), although the negative impact of high sucrose intake on some cardiac function measurements was no longer significant at this later time point.

In addition to the differences noted on LV mass and LVIDd, typical of eccentric LV hypertrophy, LFHS-fed mice exhibited increased transforming growth factor-β (TGF-β; *Tgfb1*) gene expression compared to the HFLS group (Fig. 5K). Since hypertension is a key contributor to cardiac remodeling, we next assessed systolic (Supplementary Fig. 4A), diastolic (Supplementary Fig. 4B) and mean (Supplementary Fig. 4C) arterial blood pressure at week 24. No significant modulations were noted between groups (Supplementary Fig. 4), suggesting that the observed LFHS-feeding effect on left ventricle was independent of blood pressure.

Taken together, these data indicate that high sucrose intake, independently of high blood pressure, aggravates atherosclerosis and LV enlargement, potentially contributing to cardiac dysfunction.

4. Discussion

Since wild type mice are resistant to atherosclerosis development [44] and display a different lipid profile as compared to humans, genetic manipulation targeting dyslipidemia is an indispensable tool [45]. In this study, we took advantage of the pro-atherogenic *LDLr*$^{-/-}$*ApoB*$^{100/100}$ mouse model [46] to assess the distinct roles of dietary fat and sucrose in the metabolic alterations facing a pro-atherogenic condition. Using a similar experimental strategy, our group has previously explored the distinct role of cholesterol *versus* saturated fat in T2D- and atherosclerotic-related metabolic alterations [44]. Thus, this study provides a continued follow-up into the investigative role of key dietary factors in the onset and development of cardiometabolic disorders. The principal finding of this work is that high dietary intake of sucrose promoted more severe atherosclerotic lesions and cardiac impairments than dietary fat consumption. This was linked to hepatic and visceral adipose inflammation but in the face of lower obesity-associated insulin resistance, providing novel evidence that dietary sucrose, not fat, is the main driver of atherosclerotic cardiovascular complications in an atherosclerosis-prone mouse model. Importantly, since our study was restricted to males, we encourage future research to include females to evaluate possible sex-related modulation.

While we report that high fat intake induced more obesity, insulin resistance, postprandial dyslipidemia and hepatic lipid accumulation compared to high sugar consumption, we conversely found that high sucrose augmented inflammation in metabolic and intestinal tissues, and that this was associated with increased titers against metabolic endotoxemia and a less diverse gut microbial signature. Moreover, high sucrose intake induced more atherosclerotic plaque formation and cardiac dysfunction, even in the context of low dietary fat exposure, which was concomitant with reduced cholesterol efflux capacity. These data demonstrate that excess dietary sugar is the main dietary culprit to increase CVD risk when underlying hyperlipidemia is present, and that metabolic inflammation might be a key pathogenic feature driven by high sucrose consumption in this atherogenic mouse model.

Liver is a central player of metabolic homeostasis and NAFLD is a

well-documented comorbidity of obesity [47]. However, using dyslipidemic *LDLr*$^{-/-}$ *ApoB*$^{100/100}$ mice exposed to either high fat or high sucrose intake, we were able to uncouple obesity-associated hepatic steatosis from severe hepatic inflammation and associated fibrosis. The data presented suggest that excessive consumption of fat *versus* sugar contribute differentially to NAFLD. Of note, macrovesicular steatosis, as predominantly observed in our LFHS-fed mice, is the most common type of steatosis observed in NAFLD, whereas microvesicular steatosis, characterized by smaller droplet deposition and distended hepatocytes with a foamy appearing cytoplasm, is often associated with a worse prognosis contributing to the onset of fibrosis and hepatic failure [48,49]. It is therefore intriguing that LFHS-fed mice in this study showed mild macrovascular steatosis and less microvascular fibrosis compared to their HFLS-fed counterparts, despite a greater risk of liver failure, as revealed by higher hepatic inflammation and general fibrosis score. The reason for this discrepancy remains elusive, but it is worth noting that mice fed the HFLS diet displayed hyperinsulinemia during glucose challenge and more pronounced dyslipidemia than their LFHS-fed counterparts, suggesting that both hyperinsulinemia and hyperlipidemia in HFLS-fed animals contributes to microvesicular steatosis but not necessarily hepatic inflammation *per se*.

A striking finding of this study is that LFHS feeding, despite similar caloric intake than HFLS, led to more severe atherosclerosis than high fat consumption. Recent studies have documented that high fructose intake accelerates atherosclerosis [50,51], but the specific impact of equivalent calories consumed from high sucrose *versus* high fat diets has, to the best of our knowledge, never been investigated. Using a dyslipidemic genotype, our group previously reported that high-cholesterol, but not high-fat, diet led to atheroma lesions formation, suggesting cholesterol as the main trigger in atherosclerosis [44]. Herein, the combination of dietary sucrose and cholesterol induced more severe atherosclerotic plaque formation when compared to the combination of dietary fat and cholesterol. Thus, despite cholesterol being indispensable for the onset of atherosclerosis, we demonstrated that high sucrose rather than fat intake contributes further to lesion severity. Especially considering that adding a high-fat content to the high cholesterol diet did not further increased atherosclerotic lesion formation [44]. More prominent atherosclerosis in LFHS fed animals was associated with increased inflammation in metabolic and intestinal tissues but reduced weight gain and insulin resistance as compared to HFLS-fed mice. Similarly, a diet enriched with saturated fat resulted in a worsened postprandial glycemia as compared to a high-sugar diet in overweight males [52]. Conversely, no major metabolic changes were noted among high-sugar consumers. Yet, the authors did not evaluate atherosclerosis [52]. We previously observed that the development of atherosclerotic plaques within the aorta was not related to the insulin-resistant state or body weight gain [44]. This is particularly important as both obesity and insulin resistance are generally accepted as common denominators for CVD development. Yet, our results suggest that metabolic inflammation rather than obesity drives atherosclerosis. Similarly, hypercholesterolemic *LDLr*$^{-/-}$ mice developed more atherosclerosis when fed a high-fructose diet (13% of calories from fat and 67% from carbohydrates) as compared to hyperinsulinemic western-diet-fed (42% of calories from fat, 43% from carbohydrates) mice, which was attributed to excessive VLDL-cholesterol in circulation [53]. Conversely, we found HFLS-fed mice with elevated postprandial dyslipidemia as compared to LFHS, likely reflecting a transient increase in chylomicron secretion followed a 65% lipid ingestion as compared to 14% of LFHS-fed.

Notably, the higher inflammation observed in liver, eWAT and intestine of LFHS-fed mice was not paralleled with higher aortic inflammation, suggesting that the potential mechanism underlying the severe atherosclerosis development in sucrose-fed mice is through impaired HDL function. HDL particles are mainly secreted by the liver and the gut exerting multiple vascular and anti-inflammatory activities. The most widely recognized function is the regulation of cholesterol homeostasis through cholesterol efflux from macrophage foam cells, the first key step in reverse cholesterol transport [41,54,55]. Inflammation was shown to modify HDL composition and function [56], reducing the ability of HDL to promote cholesterol efflux capacity. Similarly, liver disease was demonstrated to alter cholesterol efflux capacity of ApoB-depleted serum, which was inversely related to hepatic disease severity [57]. Likewise, we found that the greater inflammation in both liver and intestine of LFHS-fed mice paralleled reduced HDL-dependent cholesterol efflux capacity, independently of HDL levels, potentially accentuating atherosclerosis. In agreement with our findings, patients with very high HDL levels and concomitant reduced cholesterol efflux capacity paradoxically had an increased incidence of high coronary artery disease [58]. This finding is important given that dysfunctional HDL enhances atheroma lesion formation [41,54]. This might also be of potential clinical relevance, considering the recent report showing that HDL cholesterol efflux capacity is strongly associated with a future development of CVD events in the general population, independently from HDL-cholesterol levels [59]. Yet, more studies will be needed to validate these potential mechanisms at the cellular and molecular levels.

HDL also plays an important role in vascular homeostasis by activating endothelial nitric oxide synthase (eNOS), leading to enhanced production of NO, a key anti-atherogenic molecule, through a process that involves Akt activation [60]. Interestingly, the aorta of LFHS-fed mice had significantly lower expression of the genes encoding both Akt and eNOS, advocating that excessive sucrose intake not only impairs HDL cholesterol efflux capacity but also dampens eNOS activation, both of which contribute to a more severe atherosclerosis phenotype in these mice.

Substantial evidence supports the negative impact of added sugar, particularly fructose, on myocardial structural and functional integrity [61,62]. In addition to severe atherosclerosis, LFHS feeding worsens cardiac dysfunction as revealed by greater LV chamber enlargement and LV mass index as compared to HFLS-fed mice, suggesting LV eccentric hypertrophy. Increased LV mass index associated with chamber enlargement has been described as LV eccentric hypertrophy (LVEH) [63]. Similarly, fructose-rich diet has been reported to induce LV eccentric hypertrophy in rodents [61,64] and was associated with increased collagen deposition in the progressive fibrotic myocardium [62]. Intriguingly, the observed left ventricle structure disparities were not a consequence of hypertension, since both dietary groups displayed similar blood pressure levels. We also found that LFHS-induced cardiac hypertrophic was associated with increased expression of the gene encoding TGF-β a key player in cardiovascular fibrosis as an extracellular matrix modulator of the overloaded heart [65]. Thus, our findings not only demonstrate that sucrose rather than fat intake drives more severe atherosclerotic cardiovascular complications, but also corroborates that refined sugar consumption and not general overnutrition might be the main factor associated with cardiac disease in obesity in this dyslipidemic mouse model of atherosclerosis. Future studies in humans are therefore urgently warranted to define the translational impact of this conceptual finding. We further acknowledge the fact that the lack of a control healthy diet group limited some analysis interpretations, which could also be addressed in upcoming studies.

In conclusion, we believe this study describes the specific role of excessive sugar *versus* fat consumption in the context of cardiometabolic diseases. We uncoupled obesity, insulin resistance, and severe dyslipidemia from the development of NAFLD, aortic lesions and cardiac impairments, hence revealing the key role of metabolic inflammation and gut microbiota composition in these processes, providing new insights into the pathogenesis of NAFLD, atherosclerosis and CVD in diet-induced obesity.

Financial support

This work was funded by the Canadian Institutes for Health

Research (CIHR) (FDN#143247 to AM) and partly by a Dairy Research Cluster grant from Agriculture and Agri-Food Canada. AM holds a Pfizer/CIHR Research Chair in the study of insulin resistance and cardiovascular diseases. BAHJ was supported by Novo Nordisk Foundation (grant number: NNF17OC0026698). BJA holds a junior scholar award from the Fonds de recherche du Québec: Santé.

CRediT authorship contribution statement

Laís R. Perazza: Conceptualization, Methodology, Validation, Formal analysis, Investigation, Writing - original draft, Writing - review & editing, Visualization, Project administration. **Patricia L. Mitchell:** Conceptualization, Writing - review & editing, Supervision. **Benjamin A.H. Jensen:** Conceptualization, Writing - review & editing, Resources. **Noëmie Daniel:** Investigation, Writing - review & editing. **Marjorie Boyer:** Investigation, Writing - review & editing. **Thibault V. Varin:** Formal analysis, Writing - review & editing. **Rihab Bouchareb:** Investigation, Writing - review & editing. **Renato T. Nachbar:** Investigation, Writing - review & editing. **Michaël Bouchard:** Investigation, Writing - review & editing. **Mylène Blais:** Investigation, Writing - review & editing. **Andréanne Gagné:** Formal analysis, Writing - review & editing. **Philippe Joubert:** Formal analysis, Writing - review & editing. **Gary Sweeney:** Writing - review & editing. **Denis Roy:** Writing - review & editing. **Benoit J. Arsenault:** Writing - review & editing, Resources. **Patrick Mathieu:** Writing - review & editing. **André Marette:** Conceptualization, Methodology, Validation, Resources, Writing - review & editing, Supervision, Project administration, Funding acquisition.

Declaration of competing interest

The authors declared they do not have anything to disclose regarding conflict of interest with respect to this manuscript.

Acknowledgments

We would like to thank Marie-Julie Dubois, Geneviève Pilon, Yves Pouliot, Sylvie Gauthier, Martin Lessart, and Claude Asselin for their help with study design. We are also grateful to Dominic Lachance and Eric Plante that provided technical support for echocardiography data and Jose Luis Martinez that helped on the fecal DNA extraction. We also thank Valérie Dumas, Christine Dion, Christine Dallaire, Joanie Dupont-Morissette and Marion Valle for their assistance with animal protocols.

Appendix A. Supplementary data

Supplementary data to this article can be found online at https://doi.org/10.1016/j.atherosclerosis.2020.05.002.

References

[1] Philip Joseph, Darryl Leong, McKee Martin, et al., Reducing the global burden of cardiovascular disease, Part 1, Circ. Res. 121 (6) (2017) 677–694, https://doi.org/10.1161/CIRCRESAHA.117.308903.
[2] R. Ross, L. Harker, Hyperlipidemia and atherosclerosis, Science 193 (4258) (1976) 1094–1100, https://doi.org/10.1126/science.822515.
[3] E.J. Mills, B. Rachlis, P. Wu, P.J. Devereaux, P. Arora, D. Perri, Primary prevention of cardiovascular mortality and events with statin treatments, J. Am. Coll. Cardiol. 52 (22) (2008) 1769–1781, https://doi.org/10.1016/j.jacc.2008.08.039.
[4] H. Kolb, T. Mandrup-Poulsen, The global diabetes epidemic as a consequence of lifestyle-induced low- grade inflammation, Diabetologia 53 (1) (2010) 10–20, https://doi.org/10.1007/s00125-009-1573-7.
[5] A.-M. Lundsgaard, J.B. Holm, K.A. Sjøberg, et al., Mechanisms preserving insulin action during high dietary fat intake, Cell Metabol. 29 (1) (2019) 50–63, https://doi.org/10.1016/j.cmet.2018.08.022 e4.
[6] M. Dehghan, A. Mente, X. Zhang, et al., Associations of fats and carbohydrate intake with cardiovascular disease and mortality in 18 countries from five continents (PURE): a prospective cohort study, Lancet 390 (10107) (2017) 2050–2062, https://doi.org/10.1016/S0140-6736(17)32252-3.
[7] A. Astrup, A changing view on saturated fatty acids and dairy: from enemy to friend, Am. J. Clin. Nutr. 100 (6) (2014) 1407–1408, https://doi.org/10.3945/ajcn.114.099986.
[8] Y. Ma, F.J. He, Y. Yin, K.M. Hashem, G.A. MacGregor, Gradual reduction of sugar in soft drinks without substitution as a strategy to reduce overweight, obesity, and type 2 diabetes: a modelling study, Lancet Diabetes Endocrinol. 4 (2) (2016) 105–114, https://doi.org/10.1016/S2213-8587(15)00477-5.
[9] S. Basu, M. McKee, G. Galea, D. Stuckler, Relationship of soft drink consumption to global overweight, obesity, and diabetes: a cross-national analysis of 75 countries, Am. J. Publ. Health 103 (11) (2013) 2071–2077, https://doi.org/10.2105/AJPH.2012.300974.
[10] R.H. Lustig, K. Mulligan, S.M. Noworolski, et al., Isocaloric fructose restriction and metabolic improvement in children with obesity and metabolic syndrome, Obes. Silver Spring Md. 24 (2) (2016) 453–460, https://doi.org/10.1002/oby.21371.
[11] M.-R. Taskinen, S. Söderlund, L.H. Bogl, et al., Adverse effects of fructose on cardiometabolic risk factors and hepatic lipid metabolism in subjects with abdominal obesity, J. Intern. Med. 282 (2) (2017) 187–201, https://doi.org/10.1111/joim.12632.
[12] T. Jensen, M.F. Abdelmalek, S. Sullivan, et al., Fructose and sugar: a major mediator of non-alcoholic fatty liver disease, J. Hepatol. 68 (5) (2018) 1063–1075, https://doi.org/10.1016/j.jhep.2018.01.019.
[13] P. Libby, P.M. Ridker, Inflammation and atherothrombosis: from population biology and bench research to clinical practice, J. Am. Coll. Cardiol. 48 (9, Supplement) (2006) A33–A46, https://doi.org/10.1016/j.jacc.2006.08.011.
[14] P.D. Cani, R. Bibiloni, C. Knauf, et al., Changes in gut microbiota control metabolic endotoxemia-induced inflammation in high-fat diet–induced obesity and diabetes in mice, Diabetes 57 (6) (2008) 1470–1481, https://doi.org/10.2337/db07-1403.
[15] S. Ramos-Romero, M. Hereu, L. Atienza, et al., Mechanistically different effects of fat and sugar on insulin resistance, hypertension, and gut microbiota in rats, Am. J. Physiol. Endocrinol. Metab. 314 (6) (2018) E552–E563, https://doi.org/10.1152/ajpendo.00323.2017.
[16] GJ de Grooth, A.H.E.M. Klerkx, E.S.G. Stroes, A.F.H. Stalenhoef, J.J.P. Kastelein, J.A. Kuivenhoven, A review of CETP and its relation to atherosclerosis, J. Lipid Res. 45 (11) (2004) 1967–1974, https://doi.org/10.1194/jlr.R400007-JLR200.
[17] S. Chen, G. Habib, C. Yang, et al., Apolipoprotein B-48 is the product of a messenger RNA with an organ- specific in-frame stop codon, Science 238 (4825) (1987) 363–366, https://doi.org/10.1126/science.3659919.
[18] L. Johnson-Down, H. Ritter, L.J. Starkey, K. Gray-Donald, Primary food sources of nutrients in the diet of Canadian adults, Can. J. Diet Pract. Res. 67 (1) (2006) 7–13, https://doi.org/10.3148/67.1.2006.7.
[19] M. Matsuda, R.A. DeFronzo, Insulin sensitivity indices obtained from oral glucose tolerance testing: comparison with the euglycemic insulin clamp, Diabetes Care 22 (9) (1999) 1462–1470, https://doi.org/10.2337/diacare.22.9.1462.
[20] J. Folch, M. Lees, G.H. Sloane Stanley, A simple method for the isolation and purification of total lipides from animal tissues, J. Biol. Chem. 226 (1) (1957) 497–509.
[21] S.D. Parlee, S.I. Lentz, H. Mori, O.A. MacDougald, Chapter six - quantifying size and number of adipocytes in adipose tissue, in: O.A. Macdougald (Ed.), *Methods In Enzymology*. Vol 537. Methods of Adipose Tissue Biology, Part A, Academic Press, 2014, pp. 93–122, , https://doi.org/10.1016/B978-0-12-411619-1.00006-9.
[22] W. Liang, A.L. Menke, A. Driessen, et al., Establishment of a general NAFLD scoring system for rodent models and comparison to human liver pathology, PloS One 9 (12) (2014) e115922, , https://doi.org/10.1371/journal.pone.0115922.
[23] L.C. Junqueira, G. Bignolas, R.R. Brentani, Picrosirius staining plus polarization microscopy, a specific method for collagen detection in tissue sections, Histochem. J. 11 (4) (1979) 447–455.
[24] H. Puchtler, F.S. Waldrop, L.S. Valentine, Polarization microscopic studies of connective tissue stained with picro-sirius red FBA, Beitr. Pathol. 150 (2) (1973) 174–187.
[25] D.E. Kleiner, E.M. Brunt, M.V. Natta, et al., Design and validation of a histological scoring system for nonalcoholic fatty liver disease, Hepatology 41 (6) (2005) 1313–1321, https://doi.org/10.1002/hep.20701.
[26] M.H. Cooper, J.R. Miller, P.L. Mitchell, D.L. Currie, R.S. McLeod, Conjugated linoleic acid isomers have no effect on atherosclerosis and adverse effects on lipoprotein and liver lipid metabolism in apoE−/− mice fed a high-cholesterol diet, Atherosclerosis 200 (2) (2008) 294–302, https://doi.org/10.1016/j.atherosclerosis.2007.12.040.
[27] M. Boyer, P.L. Mitchell, P. Poirier, et al., Impact of a one-year lifestyle modification program on cholesterol efflux capacities in men with abdominal obesity and dyslipidemia, Am. J. Physiol. Endocrinol. Metab. 315 (4) (2018) E460–E468, https://doi.org/10.1152/ajpendo.00127.2018.
[28] Le Quang Khai, Bouchareb Rihab, Lachance Dominic, et al., Early development of calcific aortic valve disease and left ventricular hypertrophy in a mouse model of combined dyslipidemia and type 2 diabetes mellitus, Arterioscler. Thromb. Vasc. Biol. 34 (10) (2014) 2283–2291, https://doi.org/10.1161/ATVBAHA.114.304205.
[29] F.F. Anhê, R.T. Nachbar, T.V. Varin, et al., A polyphenol-rich cranberry extract reverses insulin resistance and hepatic steatosis independently of body weight loss, Mol. Metab. 6 (12) (2017) 1563–1573, https://doi.org/10.1016/j.molmet.2017.10.003.
[30] F.F. Anhê, T.V. Varin, M. Le Barz, et al., Arctic berry extracts target the gut–liver axis to alleviate metabolic endotoxaemia, insulin resistance and hepatic steatosis in diet-induced obese mice, Diabetologia 61 (4) (2018) 919–931, https://doi.org/10.1007/s00125-017-4520-z.
[31] N. Segata, J. Izard, L. Waldron, et al., Metagenomic biomarker discovery and explanation, Genome Biol. 12 (6) (2011) 1–18, https://doi.org/10.1186/gb-2011-12-6-r60.
[32] J.L. Round, S.K. Mazmanian, The gut microbiota shapes intestinal immune

responses during health and disease, Nat. Rev. Immunol. 9 (5) (2009) 313–323, https://doi.org/10.1038/nri2515.
[33] P.J. Turnbaugh, R.E. Ley, M.A. Mahowald, V. Magrini, E.R. Mardis, J.I. Gordon, An obesity-associated gut microbiome with increased capacity for energy harvest, Nature 444 (7122) (2006) 1027–1031, https://doi.org/10.1038/nature05414.
[34] L. Xiao, S.B. Sonne, Q. Feng, et al., High-fat feeding rather than obesity drives taxonomical and functional changes in the gut microbiota in mice, Microbiome 5 (1) (2017) 1–12, https://doi.org/10.1186/s40168-017-0258-6.
[35] D.A. Winer, H. Luck, S. Tsai, S. Winer, The intestinal immune system in obesity and insulin resistance, Cell Metabol. 23 (3) (2016) 413–426, https://doi.org/10.1016/j.cmet.2016.01.003.
[36] S. Mukherjee, H. Zheng, M.G. Derebe, et al., Antibacterial membrane attack by a pore-forming intestinal C- type lectin, Nature 505 (7481) (2014) 103–107, https://doi.org/10.1038/nature12729.
[37] T. Miki, O. Holst, W.-D. Hardt, The bactericidal activity of the C-type lectin RegIIIβ against Gram-negative bacteria involves binding to lipid A, J. Biol. Chem. 287 (41) (2012) 34844–34855, https://doi.org/10.1074/jbc.M112.399998.
[38] C. Bogdan, Nitric oxide and the immune response, Nat. Immunol. 2 (10) (2001) 907–916, https://doi.org/10.1038/ni1001-907.
[39] B.A. Hendrickson, R. Gokhale, J.H. Cho, Clinical aspects and pathophysiology of inflammatory bowel disease, Clin. Microbiol. Rev. 15 (1) (2002) 79–94, https://doi.org/10.1128/CMR.15.1.79-94.2002.
[40] T.C. Cullender, B. Chassaing, A. Janzon, et al., Innate and adaptive immunity interact to quench microbiome flagellar motility in the gut, Cell Host Microbe 14 (5) (2013) 571–581, https://doi.org/10.1016/j.chom.2013.10.009.
[41] R.S. Rosenson, H.B. Brewer Jr., B.J. Ansell, et al., Dysfunctional HDL and atherosclerotic cardiovascular disease, Nat. Rev. Cardiol. 13 (1) (2016) 48–60, https://doi.org/10.1038/nrcardio.2015.124.
[42] D.J. Rader, G.K. Hovingh, HDL and cardiovascular disease, Lancet 384 (9943) (2014) 618–625, https://doi.org/10.1016/S0140-6736(14)61217-4.
[43] C. Tei, L.H. Ling, D.O. Hodge, et al., New index of combined systolic and diastolic myocardial performance: a simple and reproducible measure of cardiac function–a study in normals and dilated cardiomyopathy, J. Cardiol. 26 (6) (1995) 357–366.
[44] M.-A. Laplante, A. Charbonneau, R.K. Avramoglu, et al., Distinct metabolic and vascular effects of dietary triglycerides and cholesterol in atherosclerotic and diabetic mouse models, Am. J. Physiol. Endocrinol. Metab. 305 (5) (2013) E573–E584, https://doi.org/10.1152/ajpendo.00122.2013.
[45] S. Getz Godfrey, A. Reardon Catherine, Animal models of atherosclerosis, Arterioscler. Thromb. Vasc. Biol. 32 (5) (2012) 1104–1115, https://doi.org/10.1161/ATVBAHA.111.237693.
[46] L. Powell-Braxton, M. Véniant, R.D. Latvala, et al., A mouse model of human familial hypercholesterolemia: markedly elevated low density lipoprotein cholesterol levels and severe atherosclerosis on a low-fat chow diet, Nat. Med. 4 (8) (1998) 934–938, https://doi.org/10.1038/nm0898-934.
[47] S.L. Friedman, B.A. Neuschwander-Tetri, M. Rinella, A.J. Sanyal, Mechanisms of NAFLD development and therapeutic strategies, Nat. Med. 24 (7) (2018) 908–922, https://doi.org/10.1038/s41591-018-0104-9.
[48] S. Tandra, M.M. Yeh, E.M. Brunt, et al., Presence and significance of microvesicular steatosis in nonalcoholic fatty liver disease, J. Hepatol. 55 (3) (2011) 654–659, https://doi.org/10.1016/j.jhep.2010.11.021.
[49] K.-Q. Hu, N.L. Kyulo, E. Esrailian, et al., Overweight and obesity, hepatic steatosis, and progression of chronic hepatitis C: a retrospective study on a large cohort of patients in the United States, J. Hepatol. 40 (1) (2004) 147–154, https://doi.org/10.1016/S0168-8278(03)00479-3.
[50] A. Neuhofer, B. Wernly, L. Leitner, et al., An accelerated mouse model for atherosclerosis and adipose tissue inflammation, Cardiovasc. Diabetol. 13 (2014) 23, https://doi.org/10.1186/1475-2840-13-23.
[51] N. Hutter, M. Baena, G. Sangüesa, et al., Liquid fructose supplementation in LDL-R−/− mice fed a western- type diet enhances lipid burden and atherosclerosis despite identical calorie consumption, IJC Metab. Endocro. 9 (2015) 12–21, https://doi.org/10.1016/j.ijcme.2015.10.002.
[52] S.A. Parry, F. Rosqvist, F.E. Mozes, et al., Intrahepatic fat and postprandial glycemia increase after consumption of a diet enriched in saturated fat compared with free sugars, Diabetes Care (March 2020), https://doi.org/10.2337/dc19-2331.
[53] S. Merat, F. Casanada, M. Sutphin, W. Palinski, P.D. Reaven, Western-type diets induce insulin resistance and hyperinsulinemia in LDL receptor-deficient mice but do not increase aortic atherosclerosis compared with normoinsulinemic mice in which similar plasma cholesterol levels are achieved by a fructose-rich diet, Arterioscler. Thromb. Vasc. Biol. 19 (5) (1999) 1223–1230, https://doi.org/10.1161/01.ATV.19.5.1223.
[54] E.A. Fisher, J.E. Feig, B. Hewing, S.L. Hazen, J.D. Smith, High-density lipoprotein function, dysfunction, and reverse cholesterol transport, Arterioscler. Thromb. Vasc. Biol. 32 (12) (2012) 2813–2820, https://doi.org/10.1161/ATVBAHA.112.300133.
[55] A.V. Khera, M. Cuchel, M. de la Llera-Moya, et al., Cholesterol efflux capacity, high-density lipoprotein function, and atherosclerosis, https://doi.org/10.1056/NEJMoa1001689 doi:10.1056/NEJMoa1001689.
[56] R. Birner-Gruenberger, M. Schittmayer, M. Holzer, G. Marsche, Understanding high-density lipoprotein function in disease: recent advances in proteomics unravel the complexity of its composition and biology, Prog. Lipid Res. 56 (2014) 36–46, https://doi.org/10.1016/j.plipres.2014.07.003.
[57] M. Trieb, A. Horvath, R. Birner-Gruenberger, et al., Liver disease alters high-density lipoprotein composition, metabolism and function, Biochim. Biophys. Acta 1861 (7) (2016) 630–638, https://doi.org/10.1016/j.bbalip.2016.04.013.
[58] A.P. Agarwala, A. Rodrigues, M. Risman, et al., HDL phospholipid content and cholesterol efflux capacity are reduced in patients with very high HDL-C and coronary disease, Arterioscler. Thromb. Vasc. Biol. 35 (6) (2015) 1515–1519, https://doi.org/10.1161/ATVBAHA.115.305504.
[59] Ebtehaj Sanam, Gruppen Eke G., Bakker Stephan J.L., Dullaart Robin P.F., Tietge Uwe J.F. HDL (high- density lipoprotein) cholesterol efflux capacity is associated with incident cardiovascular disease in the general population. Arterioscler Thromb Vasc. Biol. 0(0):ATVBAHA.119.312645. doi:10.1161/ATVBAHA.119.312645.
[60] C. Mineo, I.S. Yuhanna, M.J. Quon, P.W. Shaul, High density lipoprotein-induced endothelial nitric-oxide synthase activation is mediated by Akt and MAP kinases, J. Biol. Chem. 278 (11) (2003) 9142–9149, https://doi.org/10.1074/jbc.M211394200.
[61] A.-A. Bouchard-Thomassin, D. Lachance, M.-C. Drolet, J. Couet, M. Arsenault, A high-fructose diet worsens eccentric left ventricular hypertrophy in experimental volume overload, Am. J. Physiol. Heart Circ. Physiol. 300 (1) (2010) H125–H134, https://doi.org/10.1152/ajpheart.00199.2010.
[62] K.M. Mellor, J.R. Bell, M.J. Young, R.H. Ritchie, L.M.D. Delbridge, Myocardial autophagy activation and suppressed survival signaling is associated with insulin resistance in fructose-fed mice, J. Mol. Cell. Cardiol. 50 (6) (2011) 1035–1043, https://doi.org/10.1016/j.yjmcc.2011.03.002.
[63] W.H. Gaasch, D.E. Delorey, M.G.S.J. Sutton, M.R. Zile, Patterns of structural and functional remodeling of the left ventricle in chronic heart failure, Am. J. Cardiol. 102 (4) (2008) 459–462, https://doi.org/10.1016/j.amjcard.2008.03.081.
[64] D.J. Chess, W. Xu, R. Khairallah, et al., The antioxidant tempol attenuates pressure overload-induced cardiac hypertrophy and contractile dysfunction in mice fed a high-fructose diet, Am. J. Physiol. Heart Circ. Physiol. 295 (6) (2008) H2223–H2230, https://doi.org/10.1152/ajpheart.00563.2008.
[65] M. Dobaczewski, W. Chen, N.G. Frangogiannis, Transforming growth factor (TGF)-β signaling in cardiac remodeling, J. Mol. Cell. Cardiol. 51 (4) (2011) 600–606, https://doi.org/10.1016/j.yjmcc.2010.10.033.